Continent and Life Evolution

OPEN ACCESS
Article

Late Cenomanian radiolitid rudists from the Jingzhushan Formation of the northern Lhasa Terrane

Xin Rao*, Zhenglong Li, Peter W. Skelton, Shin-ichi Sano, Kai Ye and Ming Wang*
***E-mail:** xinrao@nwu.edu.cn (X.R.); wm609@163.com (M.W.)
Received 22 January 2026; Revised 12 April 2026; Accepted 15 April 2026; Published 5 June 2026
https://doi.org/10.55092/cle20260005

Graphical Abstract

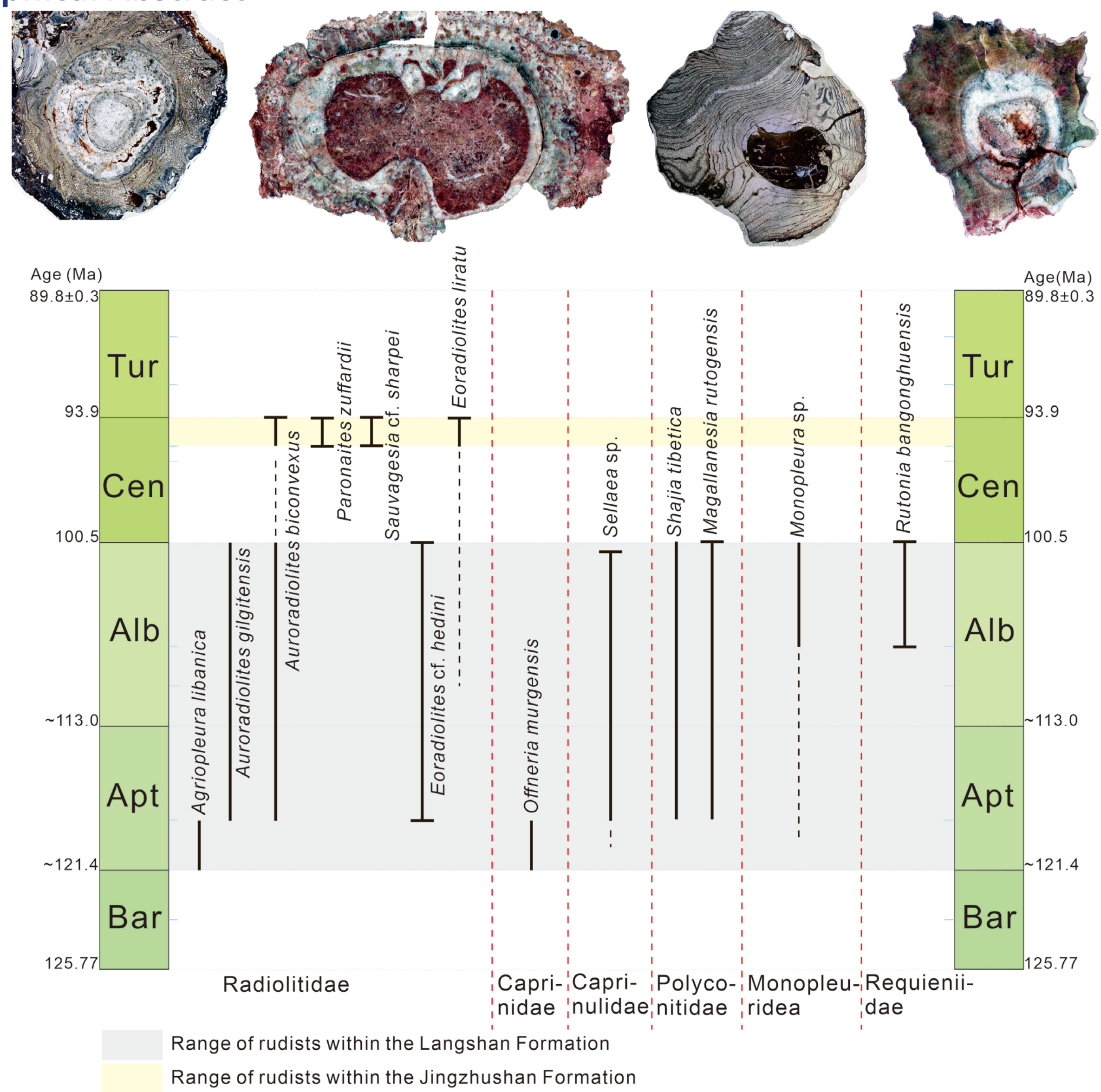

Highlights:

- First record of the late Cenomanian radiolitid association *Paronaites zuffardii*, *Eoradiolites liratus*, *Sauvagesia* cf. *sharpie* and *Auroradiolites biconvexus* in the Lhasa Terrane, eastern Tethys.
- The presence of late Cenomanian radiolitid rudists in the basal Jingzhushan Formation demonstrates that shallow-marine carbonate platform deposits existed in this unit during the late Cenomanian.
- Co-occurrence of the primitive taxon *Auroradiolites biconvexus* with more advanced radiolitids indicates a major faunal transition and radiation event of Radiolitidae in the eastern Tethys during the early Late Cretaceous.

Late Cenomanian radiolitid rudists from the Jingzhushan Formation of the northern Lhasa Terrane

Xin Rao[1,*], Zhenglong Li[2], Peter W. Skelton[3], Shin-ichi Sano[4], Kai Ye[5] and Ming Wang[2,*]

[1] State Key Laboratory of Continental Evolution and Early Life, Shaanxi Key Laboratory of Early Life and Environments, Department of Geology, Northwest University, Xi'an 710069, China

[2] College of Earth Sciences, Jilin University, Changchun 130061, China

[3] School of Environment, Earth and Ecosystem Sciences, The Open University, Milton Keynes MK7 6AA, UK

[4] Department of Earth System Science, Graduate School of Science and Engineering for Research, University of Toyama, Toyama-shi 930-8555, Japan

[5] University of Chinese Academy of Sciences, Beijing 100049, China

***E-mail:** xinrao@nwu.edu.cn (X.R.); wm609@163.com (M.W.).

Abstract: This study documents a late Cenomanian (Late Cretaceous) radiolitid rudist assemblage from the basal part of the Jingzhushan Formation in the northern Lhasa Terrane, Qinghai-Tibetan Plateau. The radiolitid fauna includes *Paronaites zuffardii*, *Eoradiolites liratus*, *Sauvagesia* cf. *sharpei*, and *Auroradiolites biconvexus*, with the first three species constituting a characteristic late Cenomanian association widely distributed in the Mediterranean Tethys and the Middle East. Their presence in the Jingzhushan Formation, previously interpreted as deposited in alluvial-fan and braided-river systems, provides definitive evidence for a shallow-marine carbonate platform environment in the northern Lhasa Terrane during the late Cenomanian. The co-occurrence of the primitive genus *Auroradiolites* with more advanced radiolitids suggests a significant faunal transition and a notable radiation event of the Family Radiolitidae in eastern Tethys during the early Late Cretaceous. These findings contribute to understanding the paleogeographic evolution of the eastern Tethys, and the stratigraphic correlation of Cenomanian shallow-water carbonates between the eastern and western Tethys.

Keywords: Lhasa Terrace; Jingzhushan Formation; late Cenomanian; Radiolitidae

1. Introduction

The Late Jurassic to Cretaceous rudist bivalves (Newell 1965) were sessile, epifaunal organisms that thrived in tropical and subtropical shallow marine carbonate platforms (Gili and Götz 2018; Skelton 2018; Skelton and Gili 2025). As the most diverse family among rudists, Radiolitidae exhibits rapid evolution and wide geographic distribution, making it particularly valuable for biostratigraphic correlation and paleoenvironmental reconstruction from the late Early Cretaceous to the Late Cretaceous (Skelton 2013a; Masse and Fenerci-Masse 2015; Philip *et al.* 2024). In the western Tethys, rudist research is well-established, providing critical insights into biostratigraphy, biogeographic correlation, paleoenvironmental reconstruction, and even hydrocarbon exploration (Cestari and Sartorio 1995; Steuber *et al.* 2016). In recent years, rudist studies in the eastern Tethys, particularly on the Qinghai-Tibetan Plateau, have made significant progress. These findings are crucial for stratigraphic correlation of Cretaceous shallow-water carbonates between the eastern and western Tethys (Rao *et al.* 2015, 2017; Sha *et al.* 2020; Gao *et al.* 2025).

The Lhasa Terrane is recognized as the last microcontinent accreted to Asia before its final collision with India in the Paleocene (Yin and Harrison 2000; Lai *et al.* 2019; Hu *et al.* 2022). Consequently, the biostratigraphy of this region is crucial for unraveling the evolution of the Tethyan realm and the early uplift history of the Tibetan Plateau (Ding *et al.* 2025; Hu *et al.* 2025). In northern and central Lhasa Terrane, two significant Cretaceous stratigraphic units are present: the Langshan Formation and the Jingzhushan Formation. The Langshan Formation is widely distributed across northern and central Lhasa Terrane, primarily consisting of limestones rich in shallow-marine fossils such as rudist bivalves and large benthic foraminifera (Xu *et al.* 2021). It was deposited mainly during the Aptian to early Cenomanian (BouDagher-Fadel *et al.* 2017; Schlagintweit and Li 2024; Ye *et al.* 2025), representing a major marine transgression across northern and central Lhasa Terrane after the initial Lhasa-Qiangtang collision (Xu *et al.* 2019). Rudist records within this formation include the early Aptian *Agriopleura libanica*–*Offneria murgensis* association (Ye *et al.* 2025) and the late Aptian–Albian *Auroradiolites biconvexus*–*Magallanesia rutogensis* assemblage (Rao *et al.* 2015, 2017).

The early Late Cretaceous Jingzhushan Formation, distributed along the northern Lhasa Terrane, has traditionally been interpreted as deposited in alluvial-fan and braided-river systems, dominated by purplish-red conglomerates and sandstones (Li *et al.* 2016). This unit has been widely regarded as marking the final retreat of the epicontinental seaway and the onset of surface uplift on the northern Lhasa Terrane (Sun *et al.* 2017; Lai *et al.* 2019). In contrast, this study reports the discovery of rudist bivalves from the basal part of the Jingzhushan Formation, providing clear evidence for a shallow-marine environment during the late Cenomanian. Through detailed systematic paleontological analysis of these rudists, we aim to firmly constrain the age of this marine interval to the late Cenomanian, and to discuss its paleobiogeographic affinities with contemporaneous Tethyan faunas.

2. Geological setting

The main body of the Qinghai-Tibetan Plateau comprises multiple terranes that amalgamated successively from north to south: the Hoh Xil–Songpan Garzê Terrane, Qiangtang Terrane, Lhasa Terrane, and Tethyan Himalayan zone. These terranes are delineated by major suture zones: the Jinshajiang suture zone (JSSZ), the Bangong Co-Nujiang suture zone (BNSZ), and the Indus-Yarlung Zangbo suture zone (IYZSZ), respectively (Yin and Harrison 2000; Pan *et al.* 2004; Wu *et al.* 2020). The Lhasa Terrane, which trends generally east–west across central Tibet, can be further subdivided into northern, central, and southern segments, separated by the Shiquanhe-Namucuo ophiolite mélange zone (SNMZ) and the Luobadui-Milashan Fault (LMF) (Figure 1a) (Zhu *et al.* 2011, 2013).

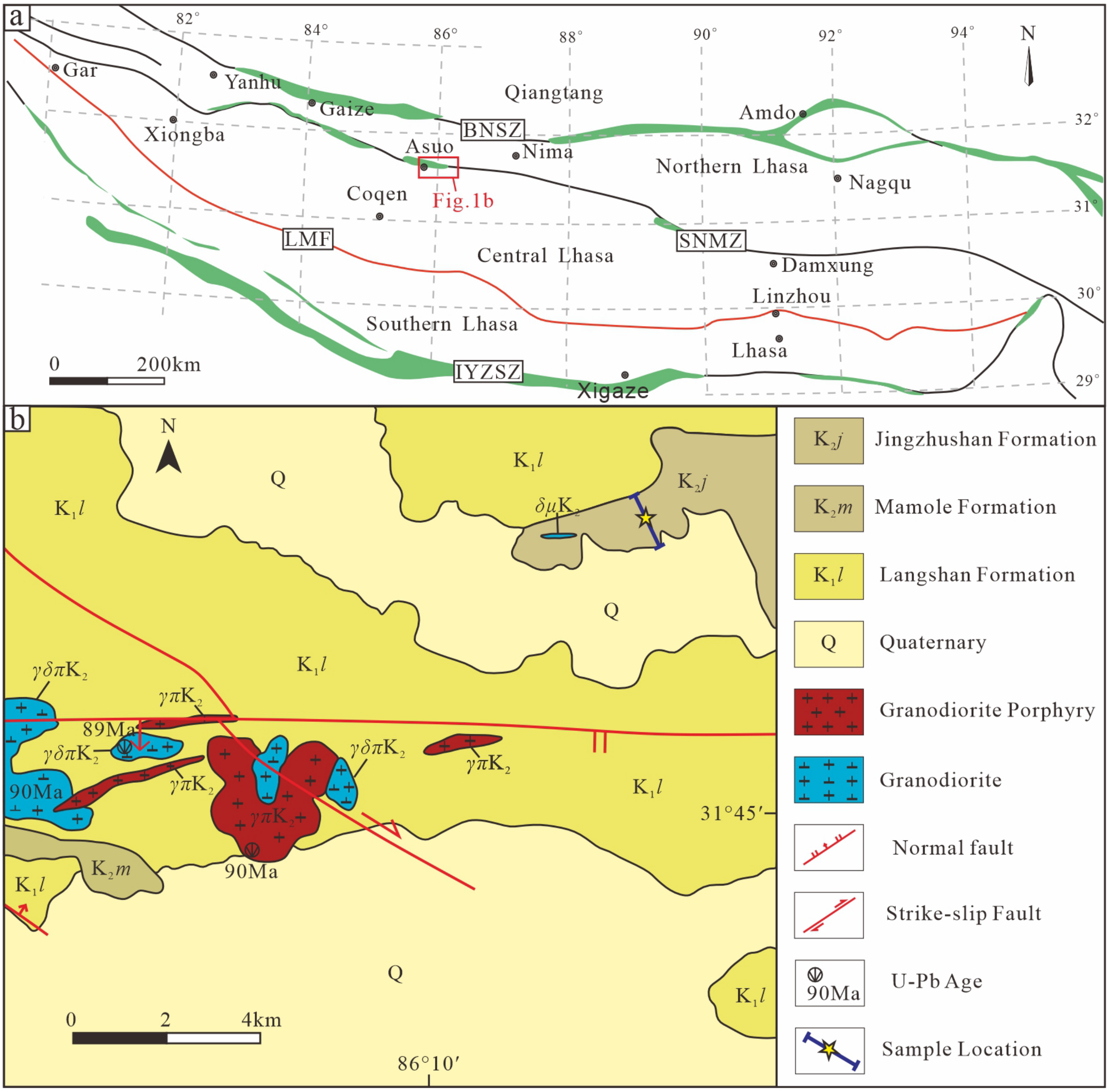

Figure 1. (a) Tectonic framework of the Lhasa Terrane, modified from (Zhu *et al.* 2011); **(b)** Simplified geological map of the Asuo area. BNSZ, Bangong Co-Nujiang suture zone; IYZSZ, Indus-Yarlung Zangbo suture zone; SNMZ, Shiquanhe-Namucuo ophiolite mélange zone; LMF, Luobadui-Milashan Fault.

The study area is situated in Asuo Township, Nyima County (Figure 1b), within the central and northern Lhasa Terrane. Cretaceous strata are widely exposed in this region and include the Aptian to Early Cenomanian Langshan Formation (Xi *et al.* 2024; Ye *et al.* 2025), the early Late Cretaceous (Cenomanian-Turonian) Mamole Formation (Zeng *et al.* 2021) and Jingzhushan Formation (Hu *et al.* 2025). The Langshan Formation is dominated by micritic and bioclastic limestones, with minor interbeds of feldspar-quartz sandstone and thin rhyolitic layers. Its fossil assemblage is dominated by rudist bivalves and orbitolinid foraminifera. The Mamole Formation consists primarily of purplish-red medium to polymictic conglomerate and fine conglomerate, locally interbedded with gravel-bearing coarse sandstone and lithic graywacke. The Jingzhushan Formation is mainly composed of purplish-red polymictic conglomerate, gravel-bearing sandstone, and siltstone, and it unconformably overlies the Langshan Formation. Magmatic activity in this area peaked during the early Late Cretaceous, as evidenced by the intrusions of adakitic granite porphyry and granodiorite porphyry at 88–90 Ma (Liu *et al.* 2018; Luo *et al.* 2019; Zeng *et al.* 2021). The radiolitid rudists described in this study were collected from the basal part of the Jingzhushan Formation at the Puga Section, which is located just north of the SNMZ (Figure 1). The basal part is composed mainly of conglomerate, with occasional thin sandstone interbeds (Figure 2a). The rudists are preserved autochthonous or parautochthonous within the conglomerate layers, mostly as upright individuals or in clusters, with their shell axes oriented nearly perpendicular to the bedding (Figure 2b–e).

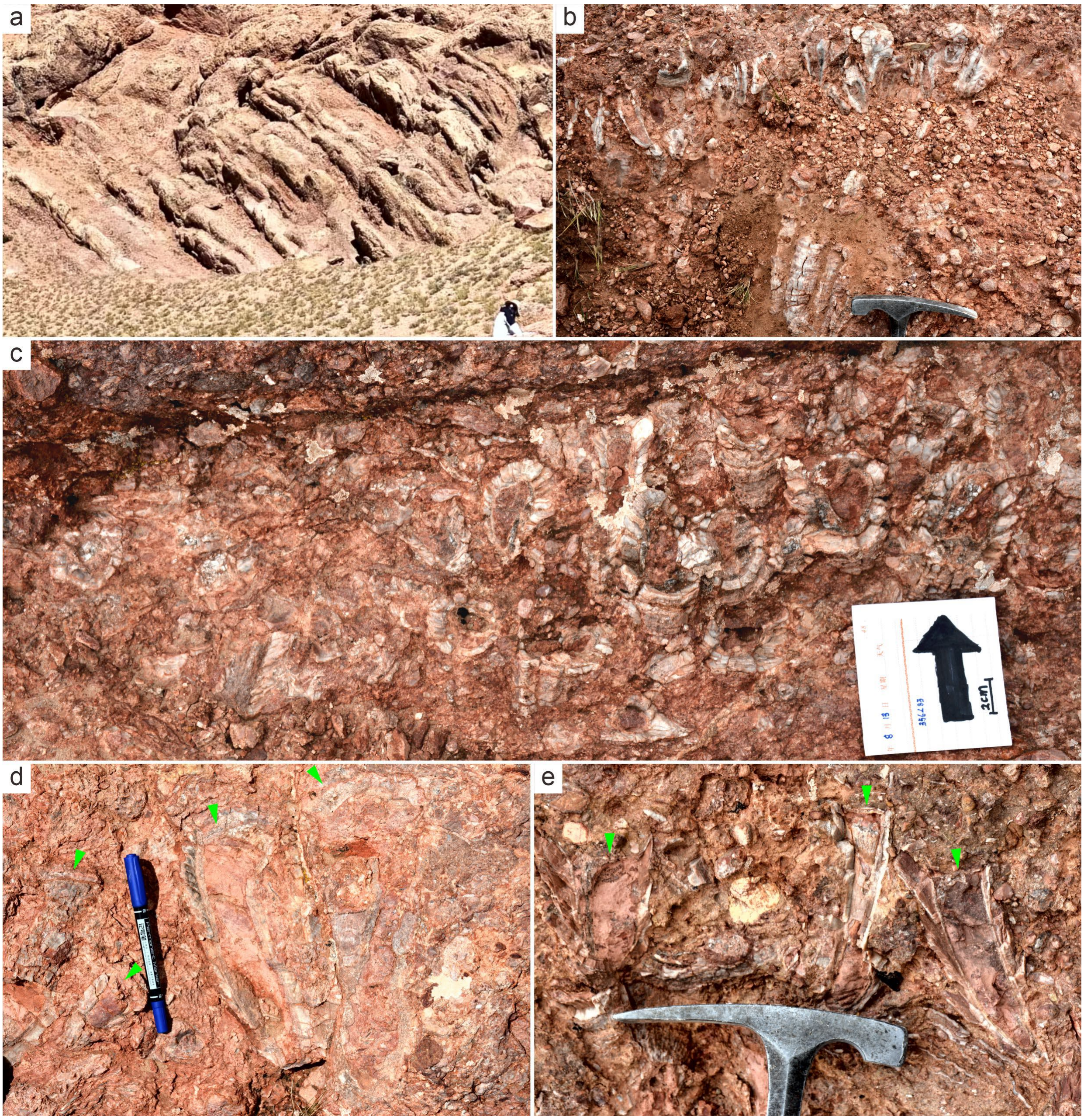

Figure 2. Field photographs of the basal part of the Jingzhushan Formation at the Puga section: **(a)** general view of the basal part of the Jingzhushan Formation; **(b–e)** side view of the radiolitid clusters, showing the growth axes of each individual nearly perpendicular to the bedding plane; green arrows in **(d, e)** point to the left valves of the articulated specimens

In addition to the radiolitid rudists, the Jingzhushan Formation at the Puga Section yields a diverse marine biota. The assemblage includes non-radiolitid rudists *Neocaprina* sp. and *Shajia tibetica*, the non-rudist bivalve *Chondrodonta joannae*, the nerineid gastropods *Neoptyxis olisiponensis* and *Simploptyxis digitalis*, the stromatoporoid sponge Coenostella sp., as well as a few poorly preserved larger benthic foraminifera. Among these taxa, *Chondrodonta joannae* and *Neoptyxis olisiponensis* are widely regarded as index fossils of the late Cenomanian (Accordi *et al.* 1982; Ayoub-Hannaa and Fürsich 2011a, 2011b; Posenato *et al.* 2020). Additionally, *Simploptyxis digitalis* has been reported from the Cenomanian of Romania (Kollmann 2014). Collectively, these fossils support a late Cenomanian age for the fossil-bearing interval of the Jingzhushan Formation.

3. Systematic palaeontology

The radiolitid fossils are heavily weathered in the field, with approximately one-third of the specimens preserved articulated (Figure 2d,e). Due to the induration of the strata, fossil collection was difficult and many specimens fractured during sampling. Consequently, most of the hand specimens are right valves and incomplete. In addition, parts of the shell ornamentation were damaged during the preparation of thin sections and polished sections.

All collected specimens are conserved in the Department of Geology, Northwest University. The classification scheme follows Skelton (Skelton 2013a, 2013b).

Abbreviations. *AVc*, antero-ventral carina; *at*, anterior tooth; *ct*, central tooth; *IB*, interband; *LV*, left valve; *ol*, outer shell layer (calcitic); *PB*, posterior radial band; *pm*, posterior myophore; *pt*, posterior tooth; *RV*, right valve; *VB*, ventral radial band.

Order Hippuritida Newell, 1965

Suborder Hippuritidina Newell, 1965

Family Radiolitidae d'Orbigny, 1847

Genus Paronaites Pons *et al.*, 2011

Type species: Radiolites zuffardii Parona, 1921, from the upper Cenomanian of Glil near Gúsbat, Homs (= Al-Khums), Libya.

Paronaites zuffardii (Parona, 1921).

Figure 3

1914 *Radiolites trigeri* Coquand, Parona, p. 21 (fide Parona, 1921).
1921 *Radiolites zuffardii* n. f. Parona, p. 19, pl. 3, Figures 3–5.
1991 *Radiolites carsicus* Caffau & Plenicar, Caffau & Plenicar, p. 266, pl. 1, Figures 1–5.
1995 *Radiolites*, Cestari & Sartorio, figures p. 35 left, figures p. 119 upper and bottom left.
1996 *Radiolites carsicus* n. sp. Caffau & Plenicar in Caffau *et al.*, p. 95, pl. 3, Figures 1–3, pl. 4, Figures 1–2, pl. 8, Figures 1–3.
2011 *Paronaites zuffardii* (Parona, 1921), Pons *et al.* Figures 5L–P, 6A–H and 7A–E.

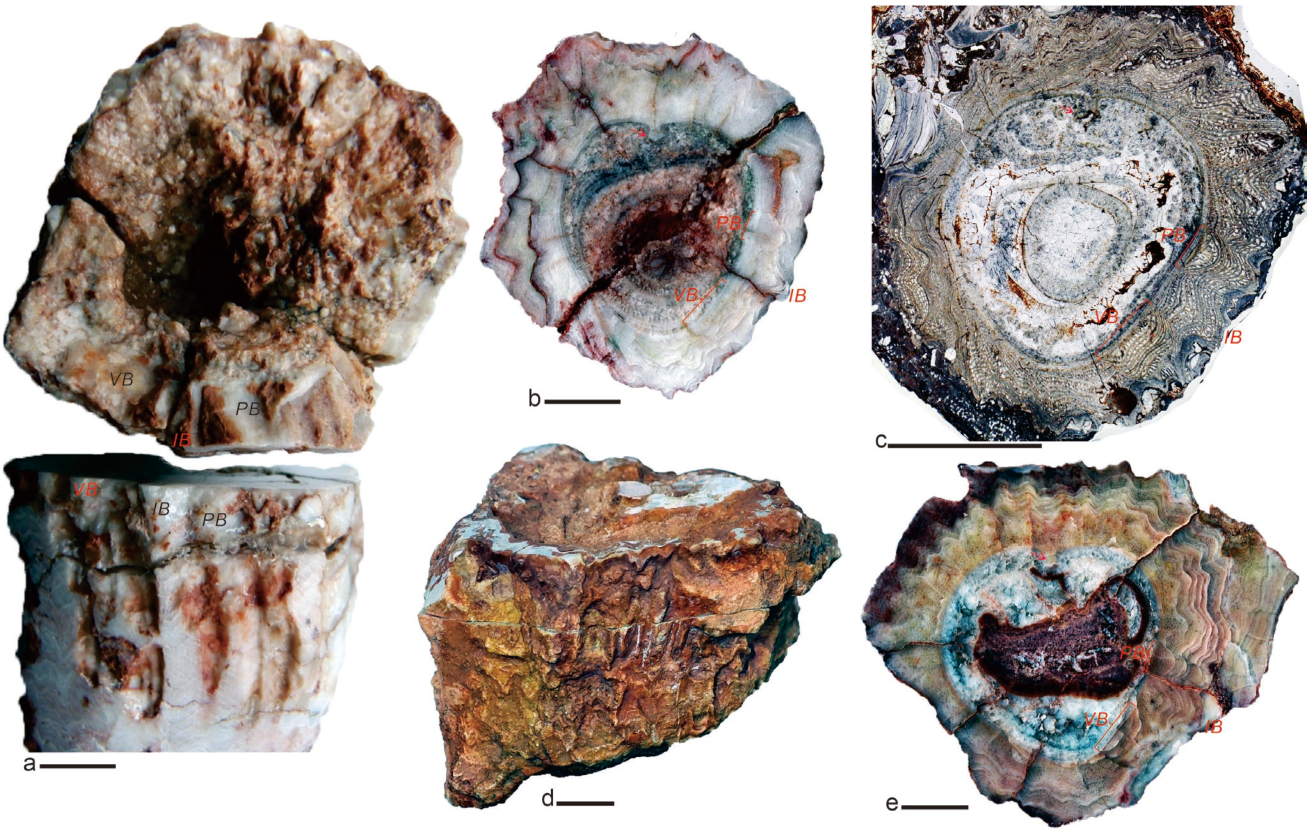

Figure 3. *Paronaites zuffardii* (Parona) from the Jingzhushan Formation of the Puga Section, Nyima County, Tibet: **(a)** right valve specimen JZS001, cut at mid-height, upper part shows the natural transverse section in adumbonal view, lower part shows the outer surface of the posterior side; **(b)** polished transverse section of JZS001 in adumbonal view; **(c)** transverse section of JZS002 in adumbonal view; **(d)** dorsal view of JZS003; **(e)** transverse section of JZS003 in adumbonal view; red arrows point to the ligament ridges. Scale bars = 10 mm.

Material. Three right valve specimens, JZS001-003.

Description. Right valve conico-cylindrical, reaching up to 90 mm in length; antero-posterior diameter ranges from approximately 23 to 55 mm. Growth lamellae gently inwardly inclined. In transverse section, costae evenly spaced and triangular (Figure 3b,c,e), matching the zig zag radial folds at the margin of the outer shell layer (Figure 3d). Radial bands not strongly defined externally, but formed by narrow, rimmed gutters on the inner margin of *ol*, producing salient ribs with V-shaped growth lines and clear cortical margin (Figure 3b,c,e). *VB* broader than *PB*, and appears dented on its central part (Figure 3b,c,e). Two radial bands separated by acutely convex, ribbed *IB* (Figure 3c). *Ol* may reach 12 mm in thickness, being thinner in the area of the radial structures than elsewhere. Fine radial ridges, normal polygonal cellular structure, and dense 'cortical' structure are commonly developed throughout the *ol*. Ligament ridge short and stubby, with slightly widened, truncated tip (red arrows in Figure 3b,c,e).

Remarks. This species was originally described as *Radiolites zuffardii* by (Parona 1921) from the upper Cenomanian of Libya, who noted its *Eoradiolites*-like radial bands and general similarity in morphology and ornamentation to several species of Radiolites. Parona (1921) also recorded the presence of a ligament ridge and pronounced radial folding of the growth lamellae, but did not examine the shell microstructure. Subsequently, Pons et *al.* (2011) revised the species based on well-preserved late Cenomanian material from Italy, and established the new genus *Paronaites* based on its unique combination of *Eoradiolites*-type radial structures, and *Radiolites*-type outer shell layer microstructure.

Our specimens from the Jingzhushan Formation are consistent with *Paronaites zuffardii* in all key morphological characters: conico-cylindrical right valve, gently inwardly inclined growth lamellae with evenly spaced triangular costae, two narrow protruding radial bands (*VB* wider than *PB*), and a short ligament ridge. A slight difference exists in the microstructure of the outer shell layer. While the Italian material exhibits a well-developed normal polygonal cellular structure throughout, our Tibetan specimens show more prominent fine radial ridges, with the polygonal cell pattern being less dominant.

The Tibetan material therefore represents the first record of *Paronaites zuffardii* in the Lhasa Terrane, extending the palaeobiogeographic range of this late Cenomanian species from the Mediterranean region to the eastern Tethys.

Genus Eoradiolites Douvillé, 1909

Type species: Radiolites davidsoni Hill, 1893, by original designation of Douvillé (1909). Upper Edwards Limestone, Albian; Belton, Texas, USA.

Eoradiolites liratus (Conrad, 1852)
Figure 4

1852 *Hippurites liratus* Conrad, Appendix, p. 234, pl. 7, Figures 47–48.
1921 *Radiolites peroni* (Choffat), Parona, p. 17, pl. 1, Figures 2 and 3.
1931 *Eoradiolites zizensis* Astre in Daguin & Astre, p. 346, pl. 19, Figures 1–5.
1934 *Eoradiolites syriacus* Conr., Blanckenhorn, p. 225, pl. 11, Figure 93.
1991 *Eoradiolites adriaticus* Caffau & Pleničar, p. 271, pl. 10, Figures 1–5, pl. 11, Figures 1–4.
1996 *Radiolites peroni* (Choffat), Caffau & Pleničar in Caffau *et al.*, p. 96, pl. 4, Figure 3.
2002 *Eoradiolites liratus* (Conrad, 1852), Steuber (with complete synonymy list until 2001). Except those citations indicated above.
non 2005 *Eoradiolites liratus* (Conrad, 1852), El Hedeni & El Sabbag, p. 555, Figures 6–9 [= *Eoradiolites schweinfurthi* (Zittel, 1883)].
2005 *Eoradiolites liratus* (Conrad, 1852), Oviedo, p. 40, Figure 29(1–5).
2011 *Eoradiolites liratus* (Conrad, 1852), Pons *et al.*, p. 651, Figures 4A–N and 5A–G.
2011 *Eoradiolites liratus* (Conrad, 1852), Zakhera, p. 419, Figures 5(1–4) and 9(1–3).
2021 *Eoradiolites liratus* (Conrad, 1852), Salama *et al.*, p. 6, Figures 4a–u and 5a,b.

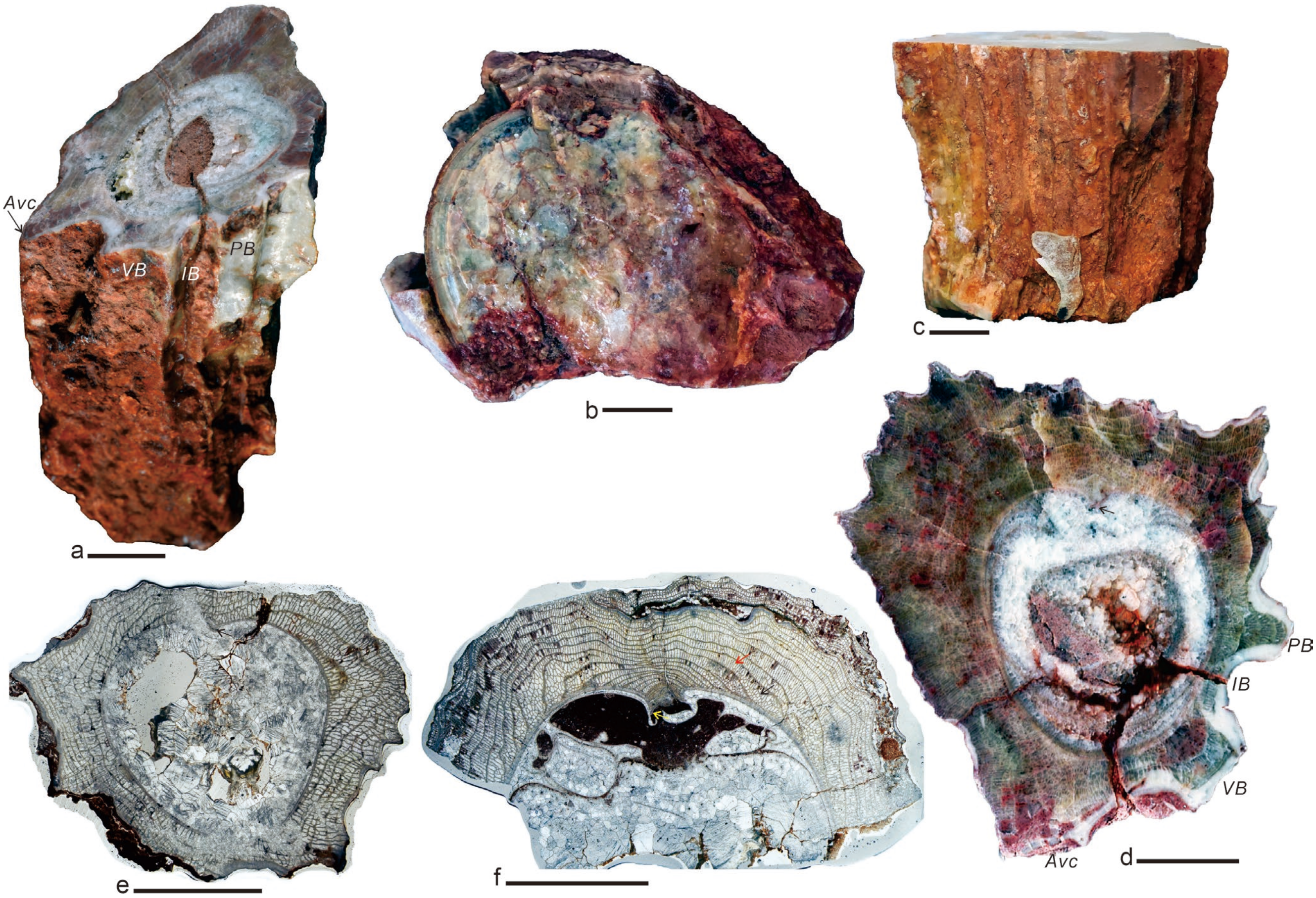

Figure 4. *Eoradiolites liratus* (Conrad) from the Jingzhushan Formation of the Puga Section, Nyima County, Tibet: **(a)** postero-ventral view of JZS005; **(b)** abumbonal view of the left valve, JZS004; **(c)** anterior view of JZS006; **(d)** transverse section of JZS006 in adumbonal view, black arrow points to the ligament ridge; **(e)** transverse section of JZS007 in abumbonal view, black arrow points to the ligament ridge; **(f)** transverse section of JZS008 in adumbonal view, yellow arrow points to the ligament ridge, red arrow indicates the radial ridge structure, black arrow indicates the normal cellular structure. Scale bars = 10 mm.

Material. One articulated specimen JZS004, and nineteen right valve specimens JZS004-023.

Description. Left valve nearly flat with concentric lamination (Figure 4b). Right valve conico-cylindrical, length of the relatively complete specimen reaches about 80 mm; antero-posterior diameter ranges from approximately 30 mm to 50 mm. Outer surface ornamented with strong, acute costae separated by broad, shallow grooves that bear smaller ribs (Figure 4c,d); both costae and grooves may be crossed at intervals by growth laminae. Two radial bands distinctly projecting, each with a slight central depression. *VB* wider than *PB*, and they separated by deeply depressed *IB* (Figure 4a,d). *AVc* evident and separated from *VB* by broad groove (Figure 4a,d). Outer shell layer varies in thickness from 5 mm to16 mm. Growth lamellae of *ol* formed by continuous radial ridges that show bifurcations (Figure 4e,f). Polygonal structure commonly developed in the inner part of the growth lamellae, resulting from increasing lateral mural connections between the radial ridges (black arrow in Figure 4f). Ligament ridge short, stubby, exhibiting triangular or Y-shaped truncation.

Remarks. The Tibetan specimens are morphologically similar to *Eoradiolites liratus* in both valve shape and radial structures, but they differ in the microstructure of the outer shell layer. Typical Mediterranean *E. liratus* possesses only a radial ridge structure (Pons *et al.* 2011), whereas the Tibetan specimens exhibit a combination of radial ridge and polygonal cellular structure. A similar mixed microstructure has been reported in *E. liratus* from the Raha Formation of western Sinai, Egypt (Zakhera 2011). Unlike the normal cellular structure observed in co-occurring *Sauvagesia* specimens, the polygonal structure of the *E. liratus* specimens is limited in distribution and arises from enhanced lateral mural connections between the radial ridges on the growth lamellae. On a single lamella, it is possible to observe a transition from dominant radial ridges (red arrow in Figure 4f) to variably developed polygonal areas (black arrow in Figure 4f) via side branching that is more complex than simple bifurcation. This mural variation in the *ol* structure of *E. liratus* likely reflects intraspecific variation, possibly of geographic, microevolutionary, or ecophenotypic origin, but is not considered here as a basis for erecting a new species.

Genus Sauvagesia Bayle, 1857

Type species: *Sphaerulites sharpei* Bayle, 1857, designated by Douvillé (1902, p. 474), from the Upper Cenomanian, Alcantara, Portugal.

Sauvagesia cf. *sharpei* (Bayle, 1857)
Figure 5

1857 *Sauvagesia sharpei* Bayle, p. 690.
2002 *Sauvagesia sharpei* (Bayle, 1857), Steuber (with complete synonymy list until 2001).
2002 *Sauvagesia sharpei* (Bayle, 1857), Chikhi-Aouimeur, p. 64, pl. 3, Figures 1–6.
2006 *Sauvagesia sharpei* (Bayle, 1857), Chikhi-Aouimeur, p. 203, Figure 6.
2010 *Sauvagesia sharpei* (Bayle, 1857), Chikhi-Aouimeur, p. 129, Figures 120–122.
2011 *Sauvagesia sharpei* (Bayle, 1857), Pons *et al.*, p. 656, Figure 8A–D.
2011 *Sauvagesia sharpei* (Bayle, 1857), Zakhera, p. 423, Figure 5(17–19).
2015 *Sauvagesia sharpei* (Bayle, 1857), Özer and Ahmad, p. 124, Figure 9A–D.
2016 *Sauvagesia sharpei* (Bayle, 1857), Özer and Ahmad, p. 149, Figure 7A–F.
2021 *Sauvagesia sharpei* (Bayle, 1857), Özer and BenYoucef, p. 10, Figure 11.
2024 *Sauvagesia* cf. *sharpei* (Bayle, 1857), Philip *et al.*, p. 12, Figure 7G.

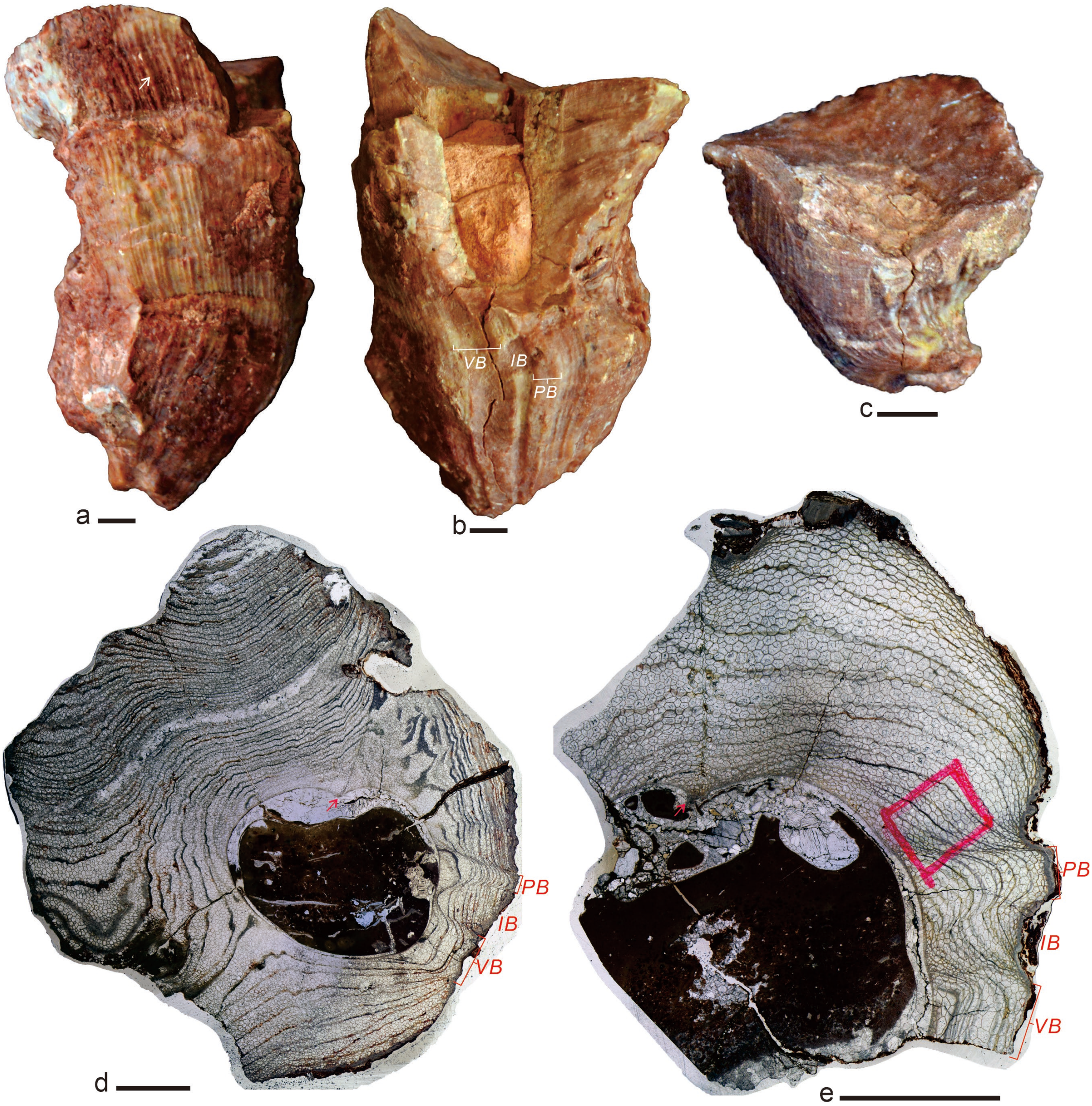

Figure 5. *Sauvagesia* cf. *sharpei* (Bayle) from the Jingzhushan Formation of the Puga Section, Nyima County, Tibet: **(a)** anterior view of JZS024, white arrow indicates the main ribs; **(b)** postero-ventral view of JZS024; **(c)** postero-ventral view of JZS025; **(d)** transverse section of JZS026 in adumbonal view, red arrow points to the ligament ridge; **(e)** transverse section of JZS027 in adumbonal view, red arrow points to the ligament ridge. Scale bars = 10 mm.

Material. Thirteen right valve specimens, JZS024-036.
Description. Shell large, reaching up to 150 mm in length. In transverse direction, shell expands rapidly during early growth, resulting in a twisted conical form in juvenile stage (Figure 5c). In adulthood, as transverse growth slows, it develops a moderately low-angle conical morphology (Figure 5a,b). Antero-posterior diameter reaches about 100 mm in the sub-commissural section. Outer surface ornamented with acute main ribs (white arrow in Figure 5a) spaced 5–10 mm apart in adult portions; between these, slightly smaller ribs are evenly spaced. Both types of ribs are intersected by growth laminae at intervals. Radial bands either slightly indented externally or slightly projecting with salient margins, widen gradually during ontogeny. *VB* about twice as wide as *PB*, and can broaden to about 15 mm in sub-commissural section. Radial bands appear smooth in majority of the specimens, though a few rare specimens exhibit finer ribbing than elsewhere on the shell. *IB* slightly concave, bearing two or three acute ribs; its width nearly equal to (Figure 5e) or slight greater than (Figure 5d) that of *PB*. Thickness of outer shell layer up to 30 mm (Figure 5b), though thinner on posterior side; fine polygonal cells occur throughout. Ligament ridge small, short, and triangular or truncated (red arrows in Figure 5d,e).
Remarks. The small triangular ligament ridge, dense ribbing, slightly concave radial bands and inter band, and thick outer shell layer with normal cellular structure observed in the studied specimens are characteristic of *Sauvagesia sharpei*. Two minor differences are noted relative to typical *S. sharpei*: (1) In *S. sharpei*, the radial bands are finely ribbed (Pons *et al.* 2011; Özer and Benyoucef 2021); whereas in the Tibetan material they are nearly smooth; (2) The outer surface of *S. sharpei* bears regular fine ribs (Pons *et al.* 2011; Özer and Benyoucef 2021), while the Tibetan right valves possess two orders of radial ribs, in which the first-order (main) ribs are only slightly more prominent than the second-order ribs, rendering the two orders nearly indistinguishable in transverse section. This condition contrasts with that of *Sauvagesia nicaisei*, whose first-order ribs are distinctly projecting and produce a conspicuous undulating pattern along the growth lamellae (Özer and Benyoucef 2021).

Genus Auroradiolites Rao *et al.*, 2015
Type species. Praeradiolites gilgitensis Douvillé, 1926a; from the upper Aptian of Kohistan, northern Pakistan.

Auroradiolites biconvexus (Yang *et al.*, 1982)
Figure 6

?1982 *Praeradiolites hedini*, Yang Zun-yi *et al.*, p. 299, pl. 1, Figure 5a–c.
1982 *Praeradiolites biconvexus*, Yang Zun-yi *et al.*, p. 299, pl. 1, Figure 4a–c.
1982 *Praeradiolites ngariensis*, Yang Zun-yi *et al.*, p. 299, pl. 1, Figures 2 and 3.
1994 *Praeradiolites gegyainensis*, Gou Zong-hai, p. 130, pl. 1, Figures 1–4.
1994 *Praeradiolites exiguus*, Gou Zong-hai, p. 130, pl. 2, Figures 1 and 2.
1994 *Praeradiolites perbellus*, Gou Zong-hai, p. 130, pl. 2, Figures 4–6.
1994 *Praeradiolites gregareus*, Gou Zong-hai, p. 131, pl. 3, Figures 6 and 7.
1997 *Praeradiolites*? sp. Masse and Gallo Maresca, p. 105, Figure 2a (= *Sphaerulites griesbachi* in Montenat *et al.*, 1982).
1998 *Praeradiolites gegyainensis*, Gou Zong-hai and Shi He, p. 261, pl. 1, Figures 1 and 2.
1998 *Praeradiolites daxungensis*, Gou Zong-hai and Shi He, p. 261, pl. 1, Figures 3 and 4.
1998 *Praeradiolites bangoinensis*, Gou Zong-hai and Shi He, p. 263, pl. 2, Figure 1.
1998 *Praeradiolites perbellus*, Gou Zong-hai and Shi He, p. 263, pl. 2, Figure 2.
1998 *Praeradiolites coquenensis*, Gou Zong-hai and Shi He, p. 263, pl. 2, Figures 3–5.
2010 *Eoradiolites gilgitensis*, Scott *et al.*, pp. 455–457, Figure 9.1–9.3.
2010 *Sphaerulites biconvexus*, Scott *et al.*, p. 457, Figure 9.4–9.7;
2015 *Auroradiolites biconvexus*, Rao Xin *et al.*, p. 407–410, Figures 3d, 4–6,7a.
2017 *Auroradiolites biconvexus*, Rao Xin *et al.*, p. 302–305, Figures 5–7.
2023 *Auroradiolites biconvexus*, Barman *et al.*, p. 7, Figure 4.

Material. Most fossils are fragmentary due to the difficulty of collecting complete specimens in the field. Many lack parts of the outer shell layer or are preserved only as shell fragments. The available material includes five articulated specimens JZS 037-041, six right valve JZS 042-047, and tens of shell fragments.
Description. Shell large, *RV* conical, with the length of incomplete specimens reaching about 110 mm; *LV* moderately domed, with convexity ranging from 5 mm (Figure 6f) to 35 mm (Figure 6a). Antero-posterior diameter of commissure may reach 150 mm. In *RV*, thickness of *ol* near the commissure can exceed 25 mm, with completely compact fibrous-prismatic microstructure observed either in natural surfaces or polished sections (Figure 6e). Growth laminae flared with distinct radial undulations that correspond to the ridges on the outer shell surface (Figure 6e). Radial bands difficult to identify in both transverse sections and on the outer surface of the shell, as the *ol* in most specimens was highly incomplete. In one exception, *PB* preserved and appears slightly indented (Figure 6g). *IB* represented by deep groove with relatively thinner *ol* compared with other parts of the shell (Figure 6g). Ligament ridge robust with typical Y-shaped termination (red arrows in Figure 6d,g). Inner shell thick, with original aragonite replaced by white to pale grey sparry calcite. Two *LV* teeth strong, straddling the narrower but prominent *RV* cardinal tooth (Figure 6d,g).

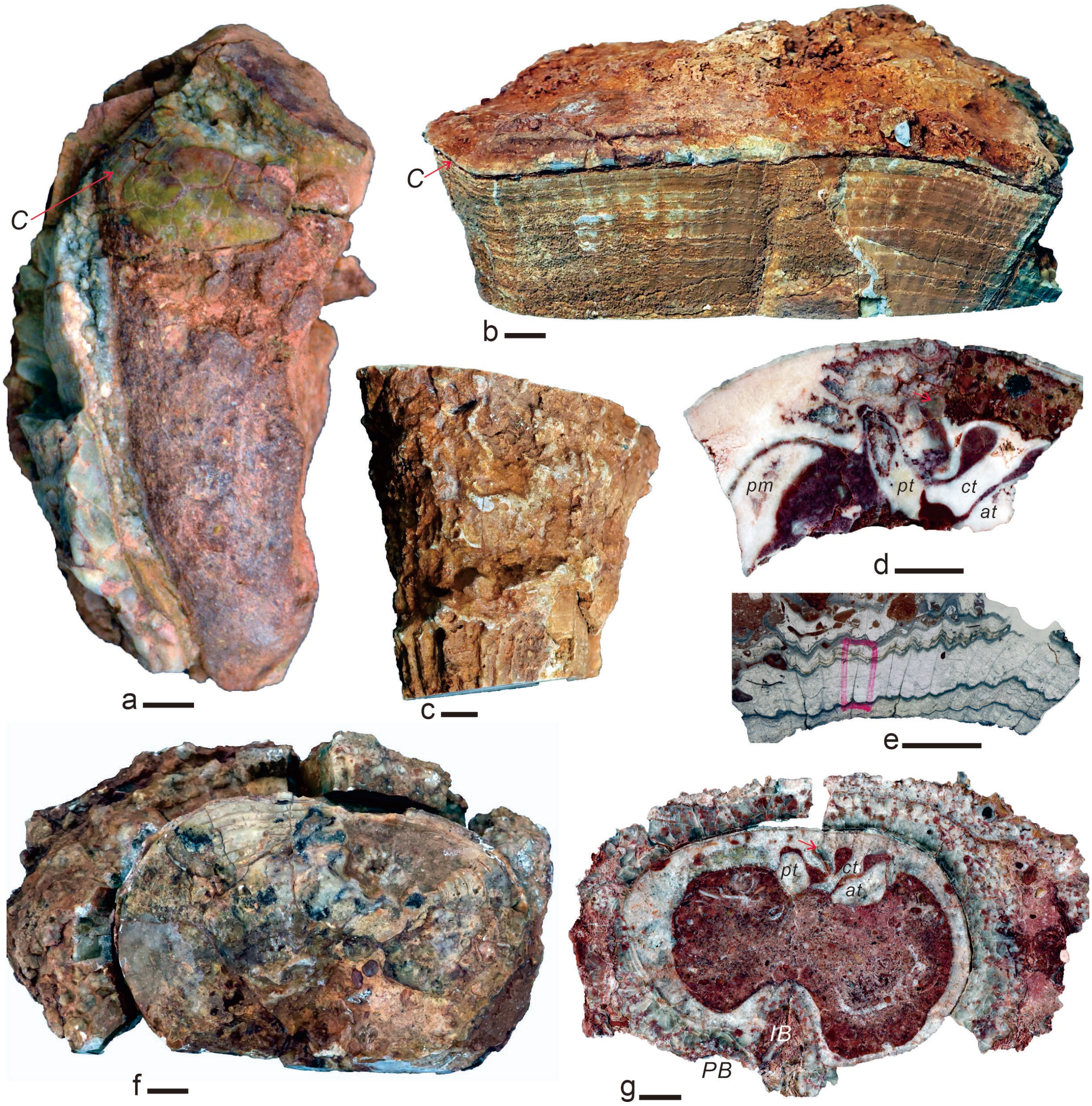

Figure 6. *Auroradiolites biconvexus* (Yang *et al.*) from the Jingzhushan Formation of the Puga Section, Nyima County, Tibet. **(a)** posterior view of articulated specimens JZS037, red arrow points to the commissure; **(b)** dorsal view of articulated specimens JZS038, red arrow points to the commissure; **(c)** anterior view of JZS042; **(d)** polished transverse section of JZS043 in abumbonal view, red arrow points to the ligament ridge; **(e)** outer shell fragment, JZS044; **(f)** abumbonal view of the left valve, JZS039; **(g)** polished transverse section of right valve in abumbonal view, red arrow points to the ligament ridge, JZS039. Scale bars = 10 mm.

4. Discussion

4.1. Recognition of marine environment in the Jingzhushan Formation

Based on their shell morphology and life habits, rudists are generally divided into three ecological morphotypes: elevators, clingers, and recumbents (Skelton and Gili 2002; Gili and Götz 2018). Elevators grew upright and became embedded in soft sediment; clingers attached to firm or hard substrates; recumbents lay prone on mobile, current-swept sea floors (Figure 7a).

In the Jingzhushan assemblage, elevators are the dominant morphotype. All radiolitid taxa described in this study are elevators, whereas the rare *Neocaprina* specimens are recumbents. Such an elevator-dominated rudist community, preserved as upright clusters, is widely interpreted as having lived in a shallow marine carbonate platform environment with relatively low energy conditions and net sediment accumulation (Figure 7f; (Ruberti and Toscano 2002; Simone *et al.* 2003; Gili and Götz 2018)). By contrast, a higher proportion of recumbents, more toppled elevator shells, and increased shell fragmentation would indicate a higher-energy carbonate platform margin setting, where currents and waves frequently reworked the sea floor (Figure 7f; Simone *et al.* 2003; Skelton and Gili 2012, 2025).

In the field, the radiolitid rudists from the basal part of the Jingzhushan Formation occur mainly as clusters, with their growth axes oriented nearly perpendicular to bedding (Figure 2b–e). Approximately one-third of the specimens are preserved with articulated valves (Figure 2d,e). Although weathering and sample preparation have caused significant damage to shell preservation, many specimens still retain delicate ornamentation, including radial ribs and commarginal growth lines (Figure 5a–c). These taphonomic features therefore provide strong evidence that the rudists were preserved autochthonously. Collectively, the evidence indicates that a normal shallow-marine carbonate platform environment existed in the Asuo area during the late Cenomanian.

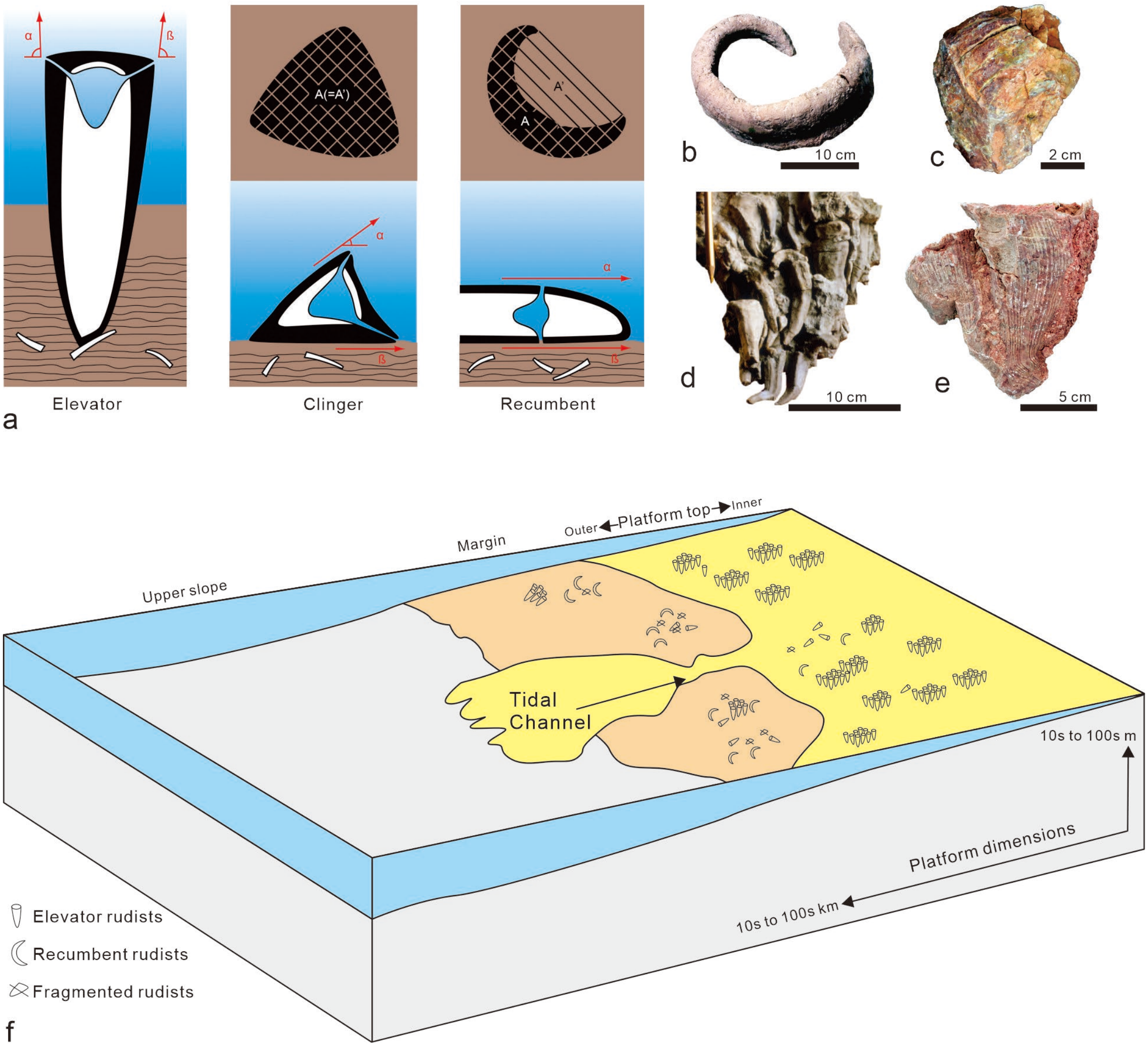

Figure 7. Rudist ecological morphotypes and carbonate platform depositional model: **(a)** ecological morphotypes of rudists (Gili and Götz 2018); **(b, c)** examples of recumbent rudists: **(b)** articulated shell of *Kimbleia albrittoni* from the Upper Albian of Texas, locality unknown ((Gili and Götz 2018), Figure 5); **(c)** articulated shell of *Neocaprina* sp. from the Jingzhushan Formation, Tibet; **(d, e)** examples of clustered elevator rudists: **(d)** *Glossomyophorus costatus* from lowermost Aptian of Sarone, Friuli, northeastern Italy ((Gili and Götz 2018), Figure 2); **(e)** *Sauvagesia* cf. *sharpei* from the Jingzhushan Formation, Tibet; **(f)** generalized model of a Cretaceous carbonate platform showing the distribution of rudist associations in the inner platform and platform margin settings (base map after (Skelton and Gili 2025), Figure 4, and (Skelton and Gili 2012), Figure 9).

4.2. The biostratigraphic implications of the radiolitid rudists from the Jingzhushan Formation

The radiolitid association documented from the Jingzhushan Formation (*Paronaites zuffardii*, *Eoradiolites liratus* and *Sauvagesia* cf. *sharpei*) indicates a late Cenomanian age. This age assignment is well supported by the known stratigraphic ranges of these taxa in other Tethyan regions (Berthou 1984; Pons *et al.* 2011; Rineau *et al.* 2021; Philip *et al.* 2024). *Paronaites zuffardii* was originally described from the upper Cenomanian of Libya (Parona 1921) and has subsequently been reported from the upper Cenomanian of Trieste, Italy (Pons *et al.* 2011). *Eoradiolites liratus* is a widely distributed species, reported from the middle-upper Cenomanian of numerous localities along the Tethyan margin, including the Middle East (e.g., Lebanon, Syria, Egypt), North Africa (e.g., Tunisia, Algeria, Morocco), and Southern Europe (e.g., Italy, Croatia) (Saber *et al.* 2009; Pons *et al.* 2011; Philip *et al.* 2024). Although recorded from the middle Cenomanian, it is most characteristic of the late Cenomanian (Philip *et al.* 2024). *Sauvagesia sharpei* is a typical late Cenomanian index species, with a broad geographic distribution across the Tethys Ocean, known from Portugal and Spain in the west, through France, Italy, the Balkans, Greece, and Turkey, to the Middle East (Lebanon, Oman, Iran) and North Africa (Morocco, Algeria, Tunisia) (Pons *et al.* 2011; Philip *et al.* 2024).

The co-occurrence of these radiolitid species, particularly *E. liratus* and *S. sharpei*, provides robust evidence for a late Cenomanian age. This association has recently been age-calibrated based on ammonite standard zonation of the Cenomanian stage from Portugal, southeastern France, and Oman, where rudist, benthic foraminifera and ammonite zones have been correlated, and the late Cenomanian age is confirmed accordingly (Philip *et al.* 2024).

Auroradiolites is a relatively primitive genus within the family Radiolitidae, characterized by a thick and entirely compact calcitic outer shell layer (Rao *et al.* 2015). *A. biconvexus* is the dominant species in the Langshan and Sangzugang formations of the Lhasa Terrane. *Auroradiolites* has previously been reported from Aptian to Albian strata in the western Pacific and southern Asia, including Hokkaido, Tibet, Ladakh, Pakistan, Afghanistan, and Iran (Rao *et al.* 2015, 2017). In contrast, the contemporaneous rudists in other Tethyan regions, such as the Mediterranean and the Middle East, are notable for the proliferation of radiolitids with cellular outer shell layer, such as *Eoradiolites* and *Archaeoradiolites* (Fenerci-Masse *et al.* 2006; Masse *et al.* 2007). By the end of the Albian, *Auroradiolites* disappeared from Hokkaido and most of southern Asia, but persisted as a relict taxon in the Karakoram and Lhasa terranes until the late Cenomanian (Xi *et al.* 2024). A pronounced radiation event of rudists occurred within the Jingzhushan Formation, characterized by the rapid evolution and high diversity of Radiolitidae (Figure 8). During this transition, the proportion of endemic taxa decreased; with only *Auroradiolites* continuing from the underlying Langshan Formation.

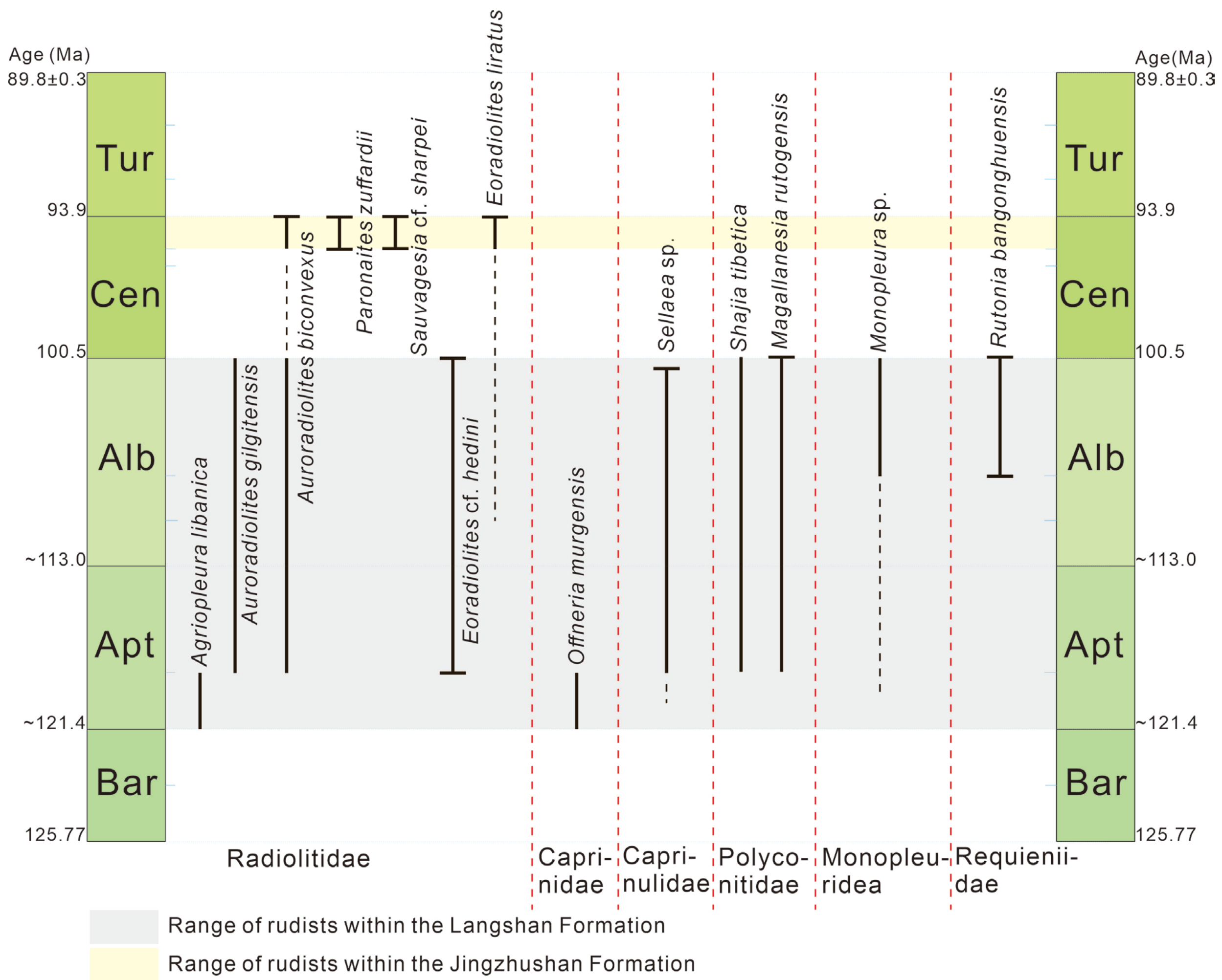

Figure 8. Stratigraphic ranges of Cretaceous rudists within the Jingzhushan Formation and Langshan Formation of the northern Lhasa Terrane (Chronostratigraphic chart follows Cohen *et al.* 2013). Bar, Barremian; Apt, Aptian; Alb, Albian; Cen, Cenomanian; Tur, Turonian.

The presence of this typical late Cenomanian Mediterranean-type radiolitid association in Tibet indicates a strong paleobiogeographic connection between the Lhasa Terrane and the western Tethyan realm during the late Cenomanian. This finding supports the presence of a marine carbonate platform environment in the northern Lhasa Terrane during the late Cenomanian, contradicting previous interpretations of the Jingzhushan Formation as entirely continental. It also provides a crucial biostratigraphic framework for regional correlation and for understanding paleogeographic evolution of the eastern Tethys during early Late Cretaceous.

5. Conclusion

The radiolitid rudist assemblage from the basal part of the Jingzhushan Formation, comprising *Paronaites zuffardii*, *Eoradiolites liratus*, *Sauvagesia* cf. *sharpei*, and *Auroradiolites biconvexus*, clearly indicates a late Cenomanian age, based on the well-established stratigraphic ranges of these species across the Tethyan realm. This typical late Cenomanian Tethyan radiolitid fauna demonstrates a strong paleobiogeographic connection between the Lhasa Terrane and the western Tethys during that period. It also confirms the existence of a shallow-marine carbonate platform environment in the northern Lhasa Terrane during the late Cenomanian, revising previous interpretations of the Jingzhushan Formation as entirely continental deposits. The co-occurrence of the three more advanced radiolitids with the primitive taxon *Auroradiolites biconvexus*, which persisted from the underlying Langshan Formation, marks a significant faunal transition and a pronounced radiation event of Radiolitidae in late Cenomanian, characterized by increased diversity and decreased endemism in the region. Therefore, this study provides a key biostratigraphic framework for stratigraphic correlation of the Lhasa Terrane with other carbonate platforms along the Tethyan margins, and for reconstructing the early Late Cretaceous paleogeographic evolution of the eastern Tethys.

Data availability statement

No supplementary or additional data were generated in this study.

Declaration of generative AI and AI-assisted technologies

The authors did not use generative AI or AI-assisted technologies in the writing of this manuscript.

Acknowledgments

This study was financially supported by the National Natural Science Foundation of China (Grant No. 42272027), special fund of Deep Earth Probe and Mineral Resources Exploration-National Science and Technology Major Project of China (No. 2025ZD1006103), the State Key Laboratory of Continental Evolution and Early Life, and the State Key Laboratory of Palaeobiology and Stratigraphy. We are grateful to Di Shen and Changsheng Yu for their invaluable field assistance.

Authors' contribution

Conceptualization, Xin Rao, Peter W. Skelton, Shin-ichi Sano and Ming Wang; methodology, Xin Rao; investigation, Xin Rao, Zhenglong Li, Kai Ye and Ming Wang; writing—original draft preparation, Xin Rao, Zhenglong Li; writing—review and editing, Peter W. Skelton, Shin-ichi Sano and Ming Wang. All authors have read and agreed to the published version of the manuscript.

Conflicts of interest

Shin-ichi Sano holds the position of Associate Editor for *Continent and Life Evolution* and has not peer reviewed or made any editorial decisions for this paper.

References

Accordi G, Carbone F, Sirna G. Relationships among tectonic setting, substratum and benthonic communities in the Upper Cretaceous of northeastern Matese (Molise, Italy). *Geol. Rom.* 1982, 21:755–793.

Ayoub-Hannaa W, Fürsich FT. Functional morphology and taphonomy of Cenomanian (Cretaceous) oysters from the eastern Sinai Peninsula, Egypt. *Palaeobiodivers. Palaeoenviron.* 2011a, 91:197–214. DOI:10.1007/s12549-011-0051-7

Ayoub-Hannaa W, Fürsich FT. Revision of Cenomanian-Turonian (Upper Cretaceous) gastropods from Egypt. *Zitteliana* 2011b, 51:115–152. DOI: 10.5282/ubm/epub.12742

Berthou PY. Albian-Turonian stage boundaries and subdivisions in the western Portuguese Basin. *Bull. Geol. Soc. Den.* 1984, 33:41–55. DOI: 10.37570/bgsd-1984-33-04

BouDagher-Fadel MK, Hu X, Price GD, Sun G, Wang JG, *et al*. Foraminiferal biostratigraphy and palaeoenvironmental analysis of the mid-Cretaceous limestones in the southern Tibetan Plateau. *J. Foraminifer. Res.* 2017, 47:188–207. DOI: 10.2113/gsjfr.47.2.188

Cestari R, Sartorio D. *Rudists and facies of the periadriatic domain*. San Donato Milanese: Agip, 1995.

Cohen KM, Kinney SC, Gibbard PL, Fan J. The ICS international chronostratigraphic chart. *Episodes* 2013, 36(3):199–204.

Ding L, Xiong Z, Tian X, He S, Zhao C, *et al*. Uplift from orogenic belts to the Tibetan Plateau: mechanisms connecting geological evolution and climate change. *Chin. Sci. Bull.* 2025, 71:494–517. DOI: 10.1360/CSB-2025-0639

Fenerci-Masse M, Masse JP, Arias C, Vilas L. *Archaeoradiolites*, a new genus from the upper Aptian of the Mediterranean region and the origin of Radiolitidae. *Palaeontology* 2006, 49:769–794. DOI: 10.1111/j.1475-4983.2006.00573.x

Gao B, Zhang Q, Rao X, Ding L. Persistence of a shallow-marine environment in western Kunlun area until early Maastrichtian. *Cretaceous Res.* 2025, 167:1–18. DOI: 10.1016/j.cretres.2024.106035

Gili E, Götz S. Paleoecology of rudists. *Treat. Online* 2018, 103:1–29. DOI: 10.17161/to.v0i0.7183

Hu X, Ma A, Wang J, Jiang J, Zhang S, *et al*. The Odyssey from marine to continental transition in the Tibetan plateau: a duet of tectonic and sea-level change. *Acta Sedimentol. Sin.* 2025, 43(5):1569–1591. DOI: 10.14027/j.issn.1000-0550.2025.046

Hu X, Ma A, Xue W, Garzanti E, Cao Y, *et al*. Exploring a lost ocean in the Tibetan Plateau: Birth, growth, and demise of the Bangong-Nujiang Ocean. *Earth Sci. Rev.* 2022, 229:104031. DOI: 10.1016/j.earscirev.2022.104031

Kollmann HA. The extinct Nerineoidea and Acteonelloidea. *Geodiversitas* 2014, 36(3):349–383. DOI: 10.5252/g2014n3a2

Lai W, Hu X, Garzanti E, Sun G, Garzione CN, *et al*. Initial growth of the Northern Lhasaplano, Tibetan Plateau in the early Late Cretaceous (ca. 92 Ma). *GSA Bull.* 2019, 131 (11–12):1823–1836. DOI: 10.1130/B35124.1

Li H, Gao C, Li Z, Zhang Z, Peng Z, *et al*. Age and tectonic significance of Jingzhushan formation in Bangong Lake area, Tibet. *Geotecton. Metallog.* 2016, 40:663–673. DOI: 10.16539/j.ddgzyckx.2016.04.004

Liu Y, Wang M, Li C, Li S, Xie C, *et al*. Late Cretaceous tectono-magmatic activity in the Nize region, central Tibet: evidence for lithospheric delamination beneath the Qiangtang–Lhasa collision zone. *Int. Geol. Rev.* 2018, 61(9):1–22. DOI:10.1080/00206814.2018.1437789

Luo A, Wang M, Li C, Xie C, Fan J, *et al*. Petrogenesis of early Late Cretaceous Asa-intrusive rocks in central Tibet, western China: post-collisional partial melting of thickened lower crust. *Int. J. Earth Sci.* 2019, 108:1979–1999. DOI: 10.1007/s00531-019-01744-4

Masse JP, Fenerci-Masse M. Evolution of the rudist bivalve *Agriopleura* Kühn (Radiolitidae, Hippuritida) from the Mediterranean region. *Palaeontology* 2015, 58(1):71–100. DOI: 10.1111/pala.12118

Masse JP, Fenerci-Masse M, Vilas L, Arias C. Late Aptian-Albian Radiolitidae from Spain and SW France. *Cretaceous Res.* 2007, 28:697–718. DOI:10.1016/j.cretres.2006.09.004

Newell ND. *Classification of the Bivalvia*. New York: American Museum Novitates, 1965. pp. 1–25.

Özer S, Benyoucef M. Late Cenomanian rudists from southern Algeria: descriptions, biostratigraphy, palaeoecology and palaeobiogeography. *Cretaceous Res.* 2021, 118:104639. DOI: 10.1016/j.cretres.2020.104639

Pan G, Zhu D, Wang L, Liao Z, Geng Q, *et al*. Bangong Lake–Nu River suture zone evidence (In Chinese). *Earth Sci. Front.* 2004, 11:371–382.

Parona CF. Fauna del Neocretacico della Tripolitania. In *Memorie per servire alla descrizione della Carta Geologica d'Italia*. Rome: Servizio Geologico d'Italia, 1921. pp. 1–21.

Philip J, Negra MH, Bachari M. Upper Cenomanian caprinulid-radiolitid rudists (Bivalvia) from the Gattar Member of Jebel el Kebar (central Tunisia): Stratigraphical implications and palaeobiogeographical relationships with coeval rudist-assemblages from carbonate platforms of the southern Tethyan margin. *Cretaceous Res.* 2024, 153(2):105713. DOI: 10.1016/j.cretres.2023.105713

Pons JM, Vicens E, Tarlao A. Cenomanian radiolitid bivalves from Malchina, Karst of Trieste, Italy. *Cretaceous Res.* 2011, 32(6):647–658. DOI: 10.1016/j.cretres.2011.03.009

Posenato R, Frijia G, Morsilli M, Moro A, Del Viscio G, *et al*. Paleoecology and proliferation of the bivalve *Chondrodonta joannae* (Choffat) in the upper Cenomanian (Upper Cretaceous) Adriatic Carbonate Platform of Istria (Croatia). *Palaeogeogr. Palaeoclimatol. Palaeoecol.* 2020, 548:109703. DOI: 10.1016/j.palaeo.2020.109703

Rao X, Skelton PW, Sano SI, Li C, Pan Y, *et al*. Evolution and palaeogeographical dispersion of the radiolitid rudist genus *Auroradiolites* (Bivalvia, Hippuritida) with descriptions of new material from Tibet and archived specimens from Afghanistan. *Pap. Palaeontol.* 2017, 3:297–315. DOI: 10.1002/spp2.1076

Rao X, Skelton PW, Sha J, Cai H, Iba Y. Mid-Cretaceous rudists from Tibet. *Pap. Palaeontol.* 2015, 1:401–424. DOI: 10.1002/spp2.1019

Rineau V, Floquet M, Villier L, Léonide P, Blénet A, *et al*. Ecological successions of rudist communities: a sedimentological and palaeoecological analysis of upper Cenomanian rudist assemblages from the South-Provence Carbonate Platform (SE France). *Sediment. Geol.* 2021, 424:105964. DOI: 10.1016/j.sedgeo.2021.105964

Ruberti D, Toscano F. Microstratigraphy and taphonomy of rudist shell concentrations in Upper Cretaceous limestones, Cilento area (central-southern Italy). *Geobios* 2002, 35(1):228–240. DOI: 10.1016/S0016-6995(02)00062-1

Saber SG, Salama YF, Scott RW, Abdel-Gawad GI, Aly MF. Cenomanian-Turonian rudist assemblages and sequence stratigraphy on the North Sinai carbonate shelf, Egypt. *GeoArabia* 2009, 14(4):113–134. DOI: 10.2113/geoarabia1404113

Schlagintweit F, Li X. Enhanced juvenile mortality of orbitolinids (larger benthic foraminifera) in the late early Aptian of the Langshan Formation, Tibet: a possible link to OAE1a? *Lethaia* 2024, 57(4):1–16. DOI: 10.18261/let.57.4.1

Sha J, Fabbi S, Cestari R, Consorti L, Scott RW, *et al*. Stratigraphic and taxonomic considerations on the Late Cretaceous rudist fauna of Aksai Chin (Western Tibet, China) from the De Filippi Collection. *Carnets Geol.* 2020, 20(13):249–272. DOI: 10.2110/carnets.2020.2013

Simone L, Carannante G, Ruberti D, Sirna M, Sirna G, *et al*. Development of rudist lithosomes in the Coniacian–Lower Campanian carbonate shelves of central-southern Italy: high-energy *vs.* low-energy settings. *Palaeogeogr. Palaeoclimatol. Palaeoecol.* 2003, 200(1–4):5–29. DOI: 10.1016/S0031-0182(03)00442-5

Skelton PW. Rudist classification: nomenclatural correction of 'Suborder Radiolitidina Skelton, 2013' to 'Suborder Hippuritidina Newell, 1965'. *Caribb. J. Earth Sci.* 2013a, 45:34.

Skelton PW. Rudist classification. *Caribb. J. Earth Sci.* 2013b, 45:9–33.

Skelton PW. Introduction to the Hippuritida (rudists): Shell structure, anatomy, and evolution. In *Treatise Online*, Lawrence: Paleontological Institute, University of Kansas, 2018. pp. 1–37.

Skelton PW, Gili E. Palaeoecological classification of rudist morphotypes. In *Proceedings of First International Conference on Rudists*, Belgrade, Yugoslavia, 2002, pp. 71–86.

Skelton PW, Gili E. Rudists and carbonate platforms in the Aptian: a case study on biotic interactions with ocean chemistry and climate. *Sedimentology* 2012, 59(1):81–117. DOI: 10.1111/j.1365-3091.2011.01292.x

Skelton PW, Gili E. Myths and models of rudist ecology. *Geologica Acta* 2025, 23:1–22. DOI: 10.1344/GeologicaActa2025.23.17

Steuber T, Scott RW, Mitchell SF, Skelton PW. Stratigraphy and diversity dynamics of Jurassic-Cretaceous Hippuritida (rudist bivalves). In *Treatise on Invertebrate Paleontology Online*. Lawrence: University of Kansas, 2016. pp. 1–17.

Sun G, Hu X, Sinclair HD. Early Cretaceous palaeogeographic evolution of the Coqen Basin in the Lhasa Terrane, southern Tibetan Plateau. *Palaeogeogr. Palaeoclimatol. Palaeoecol.* 2017, 485:101–118. DOI: 10.1016/j.palaeo.2017.06.006

Wu F, Wan B, Zhao L, Xiao W, Zhu R. Tethyan geodynamics. *Acta Petrol. Sin.* 2020, 36(6):1627–1674. DOI: 10.18654/1000-0569/2020.06.01

Xi D, Li G, Jiang S, Rao X, Jiang T, *et al*. Cretaceous integrative stratigraphy, biotas, and paleogeographical evolution of the Qinghai-Tibetan Plateau and its surrounding areas. *Sci. China Earth Sci.* 2024, 67:1229–1289. DOI: 10.1007/s11430-023-1303-2

Xu Y, Hu X, BouDagher-Fadel MK, Sun G, Lai W, *et al*. The major Late Albian transgressive event recorded in the epeiric platform of the Langshan Formation in central Tibet. *Geol. Soc. Lond. Spec. Publ.* 2019, 498:211–232. DOI: 10.1144/SP498-2019

Xu Y, Hu X, Garzanti E, BouDagher-Fadel M, Sun G, *et al*. Mid-Cretaceous carbonate accumulation in Tibet. *GSA Bull.* 2021, 134(1–2):389–404. DOI: 10.1130/B35930.1

Ye K, Rao X, Danzeng Q, Skelton PW, Gao B, *et al*. First record of early Aptian (Early Cretaceous) radiolitid *Agriopleura libanica* (Astre) from Langshan Formation, northern Lhasa Terrane: Oldest rudist bivalves in China. *Palaeoworld* 2025, 35(2). DOI: 10.1016/j.palwor.2025.201054

Yin A, Harrison TM. Geologic evolution of the Himalayan-Tibetan orogen. *Annu. Rev. Earth Planet. Sci.* 2000, 28(1):211–280. DOI: 10.1146/annurev.earth.28.1.211

Zakhera MS. Cenomanian-Turonian rudists from Western Sinai, Egypt: systematic paleontology and paleoecologyt. *Geobios* 2011, 44:409–433. DOI: 10.1016/J.GEOBIOS.2010.10.004

Zeng X, Wang M, Fan J, Luo A, Li H, *et al*. Lhasa-Qiangtang collision constraints from red beds (In Chinese). *Geol. Bull. China* 2021, 40:1428–1442.

Zhu D, Zhao Z, Niu Y, Dilek Y, Hou Z, *et al*. The origin and pre-Cenozoic evolution of the Tibetan Plateau. *Gondwana Res.* 2013, 23:1429–1454. DOI: 10.1016/j.gr.2012.02.002

Zhu D, Zhao Z, Niu Y, Mo X, Chung S, *et al*. The Lhasa Terrane: Record of a microcontinent and its histories of drift and growth. *Earth Planet. Sci. Lett.* 2011, 301:241–255. DOI: 10.1016/j.epsL.2010.11.005